Open access • Journal Article • DOI:10.1021/JP103294C

Interfacial Charge Carrier Dynamics in Core-Shell Au-CdS Nanocrystals

Ting Ting Yang, Wei Ta Chen, Yung-Jung Hsu, Kung-Hwa Wei ...+2 more authors

Institutions: National Taiwan Ocean University

Published on: 10 Jun 2010 - Journal of Physical Chemistry C (American Chemical Society)

Topics: Photoinduced charge separation and Charge carrier

Interfacial Charge Carrier Dynamics in Core−Shell Au-CdS Nanocrystals

Ting-Ting Yang,[†,‡] Wei-Ta Chen,[†,‡] Yung-Jung Hsu,*[,‡] Kung-Hwa Wei,[‡] Tai-Yuan Lin,[§] and Tai-Wei Lin[§]

Department of Materials Science and Engineering, National Chiao Tung University, Hsinchu, Taiwan 30010, Republic of China, and Institute of Optoelectronic Sciences, National Taiwan Ocean University, Keelung, Taiwan 20224, Republic of China

Received: April 13, 2010; Revised Manuscript Received: May 21, 2010

The interfacial charge carrier dynamics for core−shell Au-CdS nanocrystals with various shell thicknesses were investigated and presented. Due to the difference in band structures between Au and CdS, a pronounced photoinduced charge separation took place at the interface of Au and CdS, resulting in the electron-charged Au core and the hole-enriched CdS shell. The electron-charging of Au core in Au-CdS nanocrystals was revealed with the corresponding XPS analysis and photocurrent measurement. Time-resolved PL spectra were measured to quantitatively analyze the electron transfer event between CdS shell and Au core for Au-CdS nanocrystals. An increase in the electron-transfer rate constant was observed for Au-CdS nanocrystals with increasing shell thickness, probably due to the less pronounced electron−hole interaction of thicker CdS, which enabled a fuller extent of participation of photoexcited electrons in the charge separation process. On the other hand, the hole-enriched CdS shell of Au-CdS nanocrystals upon light illumination was characterized with a photocatalytic process. The photocatalytic activity of Au-CdS nanocrystals was found to increase with increasing shell thickness, attributable to the greater capability of light absorption achieved by the extensive growth of the CdS shell. The correlation of photocatalytic activity with the shell thickness of Au-CdS nanocrystals corresponded well with that of the electron-transfer rate constant. As compared to the relevant commercial products like N-doped P-25 TiO_2 and CdS powders, the as-synthesized Au-CdS nanocrystals exhibited superior photocatalytic performance under visible light illumination, demonstrating their potential as an effective visible-light-driven photocatalyst. Furthermore, the result of performance evaluation under natural sunlight shows that the present Au-CdS nanocrystals can be used as highly efficient photocatalysts which may practically harvest energy from sunlight.

Introduction

Modulation of charge carrier dynamics for semiconductors is important to the development of light-energy conversion systems.[1] In general, the fast recombination of charge carriers in semiconductors would diminish the resulting photoelectric conversion efficiency. To effectively gain energy from light, the photoexcited electrons and holes of semiconductors must be separated to suppress the direct recombination of them. Previous studies have shown that charge separation of semiconductors can be essentially promoted through the introduction of suitable electron acceptors, such as metals,[2] carbon derivatives,[3] and other semiconductors with appropriate band structures.[4] By adopting these composite systems, a significant enhancement in the photoconversion efficiency can be attained. For example, CdSe quantum dots can show 2−3 orders of magnitude improvement in photocurrent generation once they were capped with a molecular shell of C_{60}.[3a] This is due to the sufficiently positive reduction potential of C_{60}, which ensured a quick electron transfer from excited CdSe to C_{60} and thus the successful collection of electrons. Besides, with the attachment of CdS nanoparticles, ZnO nanowires exhibited enhanced photocatalytic activities.[4b] This enhancement resulted from the band offsets between CdS and ZnO, which may retard charge recombination to capture more charge carriers for participation in photocatalysis.

Photocatalysis is a valuable approach to practically utilize solar power. In the last two decades, much research effort has been expanded to develop semiconductor photocatalysts because of their capability of converting light energy into chemical energy. Among the various composite systems, metal/semiconductor combination is of particular interest to photocatalytic applications.[2,5] For metal/semiconductor composites, the presence of the metal−semiconductor interface may induce effective charge separation to favor the subsequent photocatalysis. The most commonly used semiconductor photocatalysts have been metal oxides like TiO_2, which exhibits ultraviolet absorption ability only due to its large bandgap energy. Many efforts have thus been made to modify TiO_2 such that it can absorb visible light to carry out photocatalytic reactions. For example, through the doping of suitable elements, an additional electronic level can be created and located in the energy gap of TiO_2, extending its light absorption range from ultraviolet to visible regions.[6] In addition to the doped TiO_2 photocatalysts, many other semiconductors that possess suitable bandgap energies are found to show fascinating photocatalytic activities upon sunlight illumination.[7] CdS is one of the most popular visible-light-driven photocatalysts since it has a bandgap energy of 2.5 eV that corresponds well with the visible light. Furthermore, its conduction band at relatively negative potential (−1.0 versus NHE)[8] offers CdS good photocatalytic activities. Until now, many

* To whom correspondence should be addressed. E-mail: yhsu@cc.nctu.edu.tw.
† These authors contributed equally to this work.
‡ National Chiao Tung University.
§ National Taiwan Ocean University.

10.1021/jp103294c
Published on Web 06/10/2010

structural forms of CdS including nanoparticles,[9] hollow nanospheres,[10] porous nanocrystals,[11] nanowires,[12] nanotubes,[13] and nanocomposites[14] have been proven effective in relevant photocatalytic processes.

We previously showed that core−shell Au-CdS nanocrystals exhibited pronounced charge carrier separation upon light illumination.[15] For Au-CdS nanocrystals, Au core can serve as an effective electron scavenger for CdS shell due to its lower Fermi energetic level (+0.5 V versus NHE) than the conduction band of CdS (−1.0 V versus NHE).[8] Consequently, the photoexcited electrons in the CdS shell would preferentially transfer to Au core, leaving positively charged holes in CdS domain to achieve charge carrier separation. In this work, we explored the interfacial charge carrier dynamics for Au-CdS nanocrystals with various shell thicknesses. By probing the emission lifetime of CdS, the electron transfer event between CdS shell and Au core for Au-CdS nanocrystals was quantitatively analyzed. A higher electron-transfer rate constant was observed for Au-CdS nanocrystals with thicker CdS shell, probably due to the less pronounced electron−hole interaction of thicker CdS that enabled a fuller extent of participation of photoexcited electrons in the charge separation process. On the other hand, the hole-enriched CdS shell of Au-CdS nanocrystals upon light illumination was characterized with a photocatalytic process. The photocatalytic activity of Au-CdS nanocrystals was found to increase with increasing shell thickness, attributable to the greater capability of light absorption achieved by the extensive growth of CdS shell. As compared to the relevant commercial products like N-doped P-25 TiO_2 and CdS powders, the as-synthesized Au-CdS nanocrystals exhibited superior photocatalytic performance under visible light illumination, demonstrating their potential as an efficient visible-light-driven photocatalyst. Furthermore, the photocatalytic performance under natural sunlight was also examined, and the result shows that the present Au-CdS nanocrystals can be used as highly efficient photocatalysts which may practically harvest energy from sunlight.

Experimental Section

Chemicals. All chemicals were analytic grade reagents and used without further purification. Special attention should be paid when dealing with the hazardous cadmium source and the highly poisonous potassium cyanide (KCN).

Preparation of Au-CdS Nanocrystals. The detailed synthetic approach and relevant characterizations of Au-CdS nanocrystals used here can be found in our previous work.[15] Briefly, Au colloids and L-cysteine-Cd^{2+} complexes (Cys/Cd) with a suitable molar ratio were mixed and allowed to undergo hydrothermal reaction at 130 °C for 6 h. The product (Au-CdS nanocrystals) was then centrifuged and washed with distilled water and ethanol to remove the remaining ions. By increasing the volumes of Cys/Cd mixed with Au colloids, Au-CdS nanocrystals with increasing shell thickness can be obtained. In this work, Au-CdS nanocrystals with three different shell thicknesses (9.0, 14.0, and 18.6 nm) were prepared and compared. The shell thickness of Au-CdS nanocrystals was determined by examining dozens of nanocrystals from the low-magnification TEM image. A number-averaged value was then calculated and represented.

Preparation of CdS Counterpart Nanocrystals. CdS counterpart nanocrystals were prepared by treating Au-CdS nanocrystals with 0.1 M KCN solution, resulting in the removal of Au core and the preservation of CdS shell (hollow structures).

Preparation of N-Doped P-25 TiO_2. N-Doped P-25 TiO_2 was prepared by annealing Degussa P-25 TiO_2 powder (1130 mg) in the mixed atmosphere of Ar (200 sccm) and NH_3 (10 sccm) at 500 °C for 2 h.[16] The x value of the product ($TiO_{2-x}N_x$) was about 0.28 as estimated from the XPS measurement.

TABLE 1: Kinetic Analysis of Emission Decay for Au-CdS Nanocrystals with Various Shell Thicknesses and Their Corresponding CdS Counterparts

entry	A_1	τ_1 (ns)	A_2	τ_2 (ns)	$\langle\tau\rangle$ (ns)	k_{et} (s^{-1})
Au-CdS, 9.0 nm	9843.3	0.37	60.9	2.58	0.46	0.36×10^9
CdS counterpart	11532.9	0.41	102.0	2.91	0.56	
Au-CdS, 14.0 nm	11539.6	0.40	110.7	2.95	0.57	0.51×10^9
CdS counterpart	9512.3	0.53	464.4	2.98	1.06	
Au-CdS, 18.6 nm	10633.5	0.39	49.4	2.99	0.48	1.42×10^9
CdS counterpart	9873.0	0.58	599.0	3.82	1.51	

Photocurrent Measurement. Photocurrent measurement for Au-CdS nanocrystals was conducted in a photoelectrochemical system under white light irradiation (xenon lamp, 250 W, with a light intensity of 100 mW/cm^2). Spin-coated film of Au-CdS nanocrystals on fluorine-doped tin oxide (FTO) substrate was used as the photoanode in the three-electrode cell which consisted of Pt counter electrode, Ag/AgCl reference electrode, and 0.1 M Na_2S redox couple.

Photoluminescence Lifetime Measurement. Time-resolved photoluminescence (PL) spectra were measured using a home-built single photon counting system. A GaN diode laser (408 nm) with a pulse duration of 50 ps was used as the excitation source. The signals collected at the excitonic emission of CdS (λ = 495 nm) were dispersed with a grating spectrometer, detected by a high-speed photomultiplier tube, and then correlated by using a single photon counting card. The emission decay data were analyzed with biexponential kinetics in which two decay components were derived. The lifetimes (τ_1 and τ_2), preexponential factors (A_1 and A_2), and intensity-average lifetime ($\langle\tau\rangle$) for Au-CdS nanocrystals and the corresponding CdS counterparts were determined and summarized in Table 1.

Photocatalytic Activity Measurement. The photocatalytic activity of Au-CdS nanocrystals was evaluated by the photodegradation of rhodamine B (RhB, $C_{28}H_{31}N_2O_3Cl$) under visible light illumination. A quartz tube with a capacity of 30 mL was used as the photoreactor vessel. The optical system used for photocatalytic reaction consisted of a xenon lamp (500 W, with a light intensity of 175 mW/cm^2) and a bandpass filter (with the bandwidth of 400−700 nm) that ensured the irradiation in the visible range. All the photocatalysis experiments were conducted at room temperature in air. Four kinds of photocatalysts including N-doped P-25 TiO_2, commercial CdS powders (Aldrich-Sigma, with the particle size of 10−20 nm), CdS counterpart, and Au-CdS nanocrystals were used and compared in the photodegradation of RhB. Typically, 5.4 mg of photocatalyst was added into 18 mL of RhB aqueous solution (1.0×10^{-5} M) in the photoreactor vessel. Prior to irradiation, the suspension was stirred in the dark for 30 min to reach the adsorption equilibrium of RhB with photocatalyst. At certain time intervals of irradiation, 1.5 mL of the reaction solution was withdrawn and centrifuged to remove photocatalyst particles. The filtrates were analyzed with a UV−visible spectrophotometer to measure the concentration variation of RhB through recording the corresponding absorbance of the characteristic peak at 553 nm. Furthermore, photodegradation of RhB (1.0×10^{-5} M) under natural sunlight by using Au-CdS nanocrystals (5.4 mg) as photocatalyst was also examined.

Characterizations. The morphology and dimensions of Au-CdS nanocrystals were examined with a high-resolution TEM (HRTEM, JEOL JEM-3000) operated at 300 kV. X-ray photoelectron spectroscopy (XPS) data were recorded with a VG

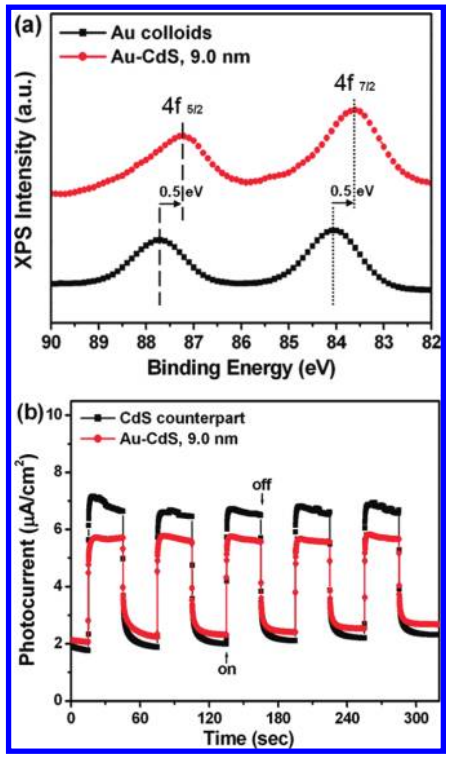

Figure 1. (a) XPS spectra of Au 4f for Au colloids and Au-CdS nanocrystals. (b) Photocurrent response of Au-CdS nanocrystal and CdS counterpart electrodes to on/off cycles of light illumination. The shell thickness of Au-CdS nanocrystals is 9.0 nm.

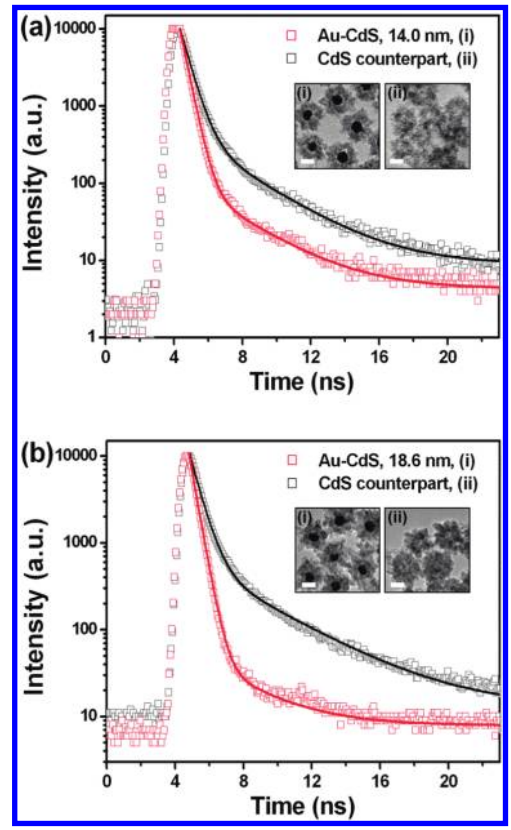

Figure 2. Time-resolved PL spectra of Au-CdS nanocrystals and CdS counterpart with the shell thickness of (a) 14.0 and (b) 18.6 nm. The fitting results (solid curves) were also included for comparison. Insets show the corresponding TEM images and the scale bar is 20 nm.

Scientific Microlab 350 electron spectrometer using Mg Kα ($h\nu = 1253.6$ eV) as X-ray source under a base pressure of 1.0×10^{-9} Torr. The spectrum resolution of XPS was 0.1 eV, and the pass energy for survey and fine scans was 40 eV. All the binding energies were calibrated by C 1s at 284.6 eV. Photocurrent signals were recorded with a Keithley 2400 semiconductor analyzer. UV−visible spectra were collected with a Hitachi U-3900H at room temperature under ambient atmosphere.

Results and Discussion

First, core−shell nanocrystals of Au-CdS were prepared in a hydrothermal process by using the presynthesized Au colloids and Cys/Cd complexes as the starting materials. The formation of Au-CdS nanocrystals involved the binding of Cys/Cd complexes toward Au nanoparticles, followed by the decomposition of Cys/Cd in the hydrothermal reaction and the subsequent growth of CdS onto the surfaces of Au. By suitably modulating the experimental parameters such as the volumes of Cys/Cd added, a controllable shell thickness of Au-CdS nanocrystals can be achieved. In this work, Au-CdS nanocrystals with three different shell thicknesses (9.0, 14.0, and 18.6 nm) were prepared and compared. The present Au-CdS nanocrystals provide an ideal platform to study the interfacial charge carrier dynamics for metal−semiconductor core−shell heterostructures. Due to the difference in band structures between Au and CdS, a pronounced photoinduced charge separation took place at the interface of Au and CdS, resulting in the electron-charged Au core and the hole-enriched CdS shell. The electron-charging of Au core in Au-CdS nanocrystals can be revealed with the corresponding XPS analysis and photocurrent measurement. As shown by the XPS spectra of Figure 1a, a binding energy of 84.1 eV of Au $4f_{7/2}$ peak was found for pure Au colloid sample, which is in good agreement with the value of bulk metallic Au.[17] However, a negative binding energy shift of around 0.5 eV of Au $4f_{7/2}$ peak was observed for Au-CdS nanocrystals, indicating a significant difference in electronic structures between Au and CdS and a strong electronic interaction therein.[18] A similar phenomenon was reported in the Au-SnO_2 core−shell nanocrystal system, in which the binding energy shift of Au 4f was attributed to the effective electron transfer from SnO_2 to Au.[19] Here we ascribed the negative binding energy shift of Au 4f observed in Au-CdS nanocrystals to the electron-charging of Au core that resulted from the occurrence of charge separation. To further elucidate the effect of Au on the charge separation of CdS for the present core−shell nanocrystals, we compared the photocurrent response of Au-CdS nanocrystal and CdS counterpart electrodes by inserting them in a photoelectrochemical cell. Note that the CdS counterpart was composed of CdS hollow structures, which were prepared by dissolving the Au core of Au-CdS nanocrystals.[15] Figure 1b depicts the photocurrent generation for Au-CdS nanocrystal and CdS counterpart electrodes subjected to the white light irradiation. Both electrodes showed prompt response to the on/off cycles of light illumination, demonstrating the effective charge transfer and successful electron collection for the samples within the photoelectrochemical cell. More importantly, Au-CdS nanocrystals exhibited lower photocurrents than CdS counterpart upon light irradiation. We believed that the significant electron transfer from CdS shell to Au core accounted for such an evident photocurrent depression found in Au-CdS nanocrystals.

If the observed photocurrent depression as well as the XPS binding energy shift for Au-CdS nanocrystals indeed involved the electron transfer from CdS to Au, we should be able to reveal this event in the excitonic emission decay profile of CdS. Figure 2 represents the time-resolved PL spectra for two Au-CdS samples with different shell thicknesses. The emission decay

data were analyzed with biexponential kinetics in which two decay components were derived. For Au-CdS nanocrystals with the shell thickness of 14.0 nm, emission lifetimes of both components were shorter than those of the corresponding CdS counterpart ($\tau_1 = 0.40$ ns, $\tau_2 = 2.95$ ns for Au-CdS versus $\tau_1 = 0.53$ ns, $\tau_2 = 2.98$ ns for CdS counterpart). The intensity-average lifetime was then calculated to make an overall comparison of the emission decay behavior.[20] The difference in the average emission lifetime between Au-CdS ($\langle\tau\rangle = 0.57$ ns) and CdS counterpart ($\langle\tau\rangle = 1.06$ ns) indicates the emergence of a nonradiative pathway from the interaction between CdS and Au. This proposition can be confirmed by the emission quenching of CdS observed for Au-CdS sample.[15] Such difference became more noticeable as the shell thickness of Au-CdS nanocrystals further increased to 18.6 nm ($\langle\tau\rangle = 0.48$ ns for Au-CdS versus $\langle\tau\rangle = 1.51$ ns for CdS counterpart), inferring a much more significant electronic interaction between CdS and Au. If electron transfer from CdS to Au was the predominant process that dictated the emission quenching of CdS, we can then estimate the electron-transfer rate constant (k_{et}) of Au-CdS nanocrystals from the emission lifetime data by the following equation:

$$k_{et} = \frac{1}{\langle\tau\rangle}(\text{Au-CdS}) - \frac{1}{\langle\tau\rangle}(\text{CdS})$$

Using the lifetime values listed in Table 1, we obtained the electron-transfer rate constants as 0.36×10^9, 0.51×10^9, and 1.42×10^9 s^{-1} for Au-CdS nanocrystals with the shell thickness of 9.0, 14.0, and 18.6 nm, respectively.

It should be noted that the electron-transfer rate constant of Au-CdS nanocrystals increased with increasing shell thickness. The less pronounced interaction between electrons and holes in the thicker CdS shell may contribute to such an increase in electron-transfer rate constant for Au-CdS nanocrystals with increasing shell thickness. We noticed that the emission lifetimes of the three CdS counterpart samples were substantially different, with CdS of larger characteristic size (thickness) showing longer emission lifetime, as can be seen in Table 1. This size-dependent correlation of exciton lifetime has been widely reported for CdS nanocrystals.[21] It is generally believed that the significant interaction between electrons and holes, which is due to the confinement of electrons and holes in a particle of reduced size, may induce additional pathways for nonradiative recombination.[22] A shortened exciton lifetime would consequently be observed for CdS nanocrystals with reduced size. The electron−hole interaction in small particles is related to the trapping of excitons by the abundant surface states that may further act as alternative sites for nonradiative charge recombination.[23] For the present Au-CdS nanocrystals, it is reasonable to presume a less pronounced electron−hole interaction for Au-CdS with thicker CdS shell since they possessed a larger characteristic size of CdS and thus a smaller number of surface states. Such less pronounced electron−hole interaction in fewer surface states prohibited charge carriers from being consumed in nonradiative recombination, which further enabled a fuller extent of participation of photoexcited electrons in the charge separation process. Accordingly, an increase in the electron-transfer rate constant was observed for Au-CdS nanocrystals with increasing shell thickness.

Since Au-CdS nanocrystals exhibited pronounced charge separation upon light illumination, it is worth studying the potential application that this property may bring. Owing to the effective electron transfer from CdS shell to Au core, photo-

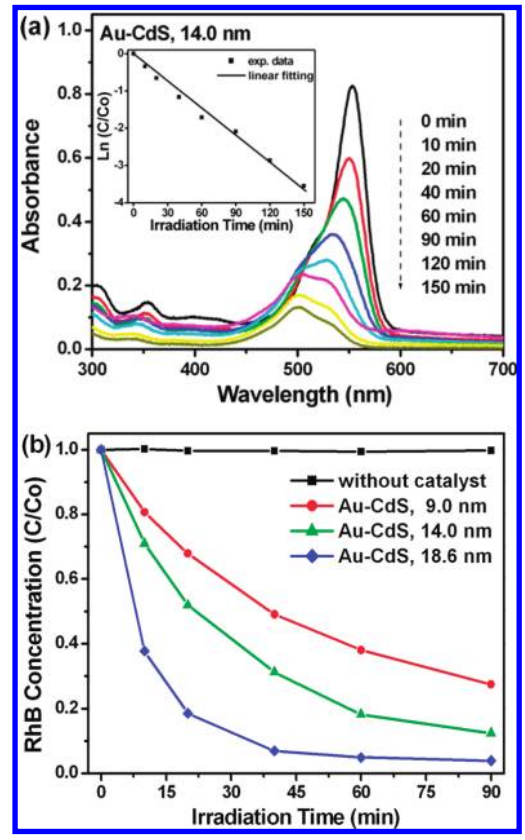

Figure 3. (a) Absorption spectra of RhB solutions under different irradiation times by using Au-CdS nanocrystals with the shell thickness of 14.0 nm. Inset: The $\ln(C/C_o)$ versus irradiation time plot with the fitting result included. (b) C/C_o versus irradiation time plots for RhB photodegradation without any catalyst and in the presence of Au-CdS nanocrystals with various shell thicknesses.

generated holes of an abundant amount were existent in CdS shell and would transfer to the surfaces of Au-CdS nanocrystals. These highly reactive holes could oxidize water to produce hydroxyl radicals that can further decompose organic pollutants through an oxidation process. A spectacular capability of photocatalytic oxidation is therefore expected at the surfaces of Au-CdS nanocrystals. A series of photocatalysis experiments were performed in this work to investigate the photocatalytic properties of the as-synthesized Au-CdS nanocrystals. RhB, a typical dye that can be decomposed by hydroxyl radicals,[24] was used as the test pollutant to monitor the photocatalytic oxidation progress for Au-CdS nanocrystals. The time-dependent UV−visible spectra of RhB solutions under visible light illumination in the presence of Au-CdS nanocrystals with a shell thickness of 14.0 nm were first shown in Figure 3a. It can be seen that the intensity of the characteristic absorption peak at 553 nm decreased dramatically with the irradiation time. Besides, a concomitant blue shift in the absorption maximum was observed after the solution was irradiated for 20 min. It is well-known that the photodegradation of RhB undergoes two competitive processes.[25] One is the destruction of dye chromogen, which is characteristic of the loss of absorbance at 553 nm. The other is the N-demethylation reaction that produces a series of N-demethylated intermediates, accompanied by a blue shift in the absorption maximum from 553 to 498 nm. In the current case, RhB concentration was determined by referring to the absorbance of the characteristic peak at 553 nm. To quantitatively understand the reaction kinetics of RhB photodegradation for our samples, we analyzed the normalized concentration of RhB (C/C_o) as a function of irradiation time. As shown in the inset

of Figure 3a, an exponential decay of RhB concentration with the irradiation time was evident for Au-CdS nanocrystal photocatalyst. The photodegradation process was then fit to pseudo-first-order reaction, in which the value of the apparent rate constant (k_{RhB}) is equal to the slope of the fitting line according to the following expression:[26] $\ln(C/C_o) = -k_{RhB}t$, where C_o and C are the concentrations of RhB at initial and at a certain irradiation time t, respectively.

For Au-CdS nanocrystals with a shell thickness of 14.0 nm, k_{RhB} is found to be 0.026 min^{-1}. The mechanism for RhB photodegradation by using Au-CdS nanocrystal photocatalyst can be described by the following four pathways:

$$\text{Au-CdS} + h\nu \rightarrow \text{Au}(e^-)\text{-CdS}(h^+) \quad (1)$$

$$\text{Au}(e^-)\text{-CdS}(h^+) + H_2O \rightarrow \text{Au}(e^-)\text{-CdS} + H^+ + {}^\bullet OH \quad (2)$$

$$\text{RhB} + {}^\bullet OH \rightarrow \text{oxidation products} \quad (3)$$

$$\text{Au}(e^-)\text{-CdS} + O_2 \rightarrow \text{Au-CdS} + {}^\bullet O_2^- \quad (4)$$

Under visible light illumination, charge separation occurred within Au-CdS nanocrystals, resulting in an electron-charged Au core and a hole-enriched CdS shell (eq 1). Subsequently, the photogenerated holes transferred to the surfaces of nanocrystals and reacted with water to produce hydroxyl radicals (eq 2). RhB molecules were then decomposed by hydroxyl radicals through an oxidation process (eq 3). Once the photogenerated holes were depleted in photocatalysis, Au-CdS nanocrystals underwent a Fermi level equilibration due to the accumulation of photoexcited electrons.[27] Note that experiments of RhB photodegradation were conducted in air. The exposure to air during the operation of photocatalysis can discharge the accumulating electrons of Au-CdS nanocrystals to the dissolved oxygen,[5a,28] which resulted in a neutralized state of nanocrystals that are allowed for further photoexcitation (eq 4).

The photocatalytic performance of Au-CdS nanocrystals with three various shell thicknesses was then compared in Figure 3b. It should be noted that experiment in the absence of photocatalyst showed almost no RhB photodegradation, implying that the self-photolysis of RhB is negligible under visible light illumination. For Au-CdS nanocrystals with a shell thickness of 9.0 nm, about 50% of RhB was degraded after 40 min of irradiation. A higher extent of RhB photodegradation to around 70% at the same irradiation time was achieved when using Au-CdS nanocrystals with a thicker shell of 14.0 nm. For Au-CdS nanocrystals with the shell thickness of 18.6 nm, RhB was almost completely decomposed after 40 min of irradiation. From the above observations, we concluded that the photocatalytic activity of Au-CdS nanocrystals was enhanced with increasing shell thickness. This is mainly a result of the extensive growth of CdS shell in Au-CdS nanocrystals. With increasing shell thickness, a raised ratio in the amount of CdS to Au was attained, leading to a greater capability of light absorption for Au-CdS nanocrystals and thus the generation of more charge carriers. This argument can be verified by the fact that the excitonic absorption of CdS for Au-CdS nanocrystals turned significant with increasing shell thickness.[15] Consequently, a higher number of photoexcited charge carriers was expected for Au-CdS nanocrystals with larger shell thickness, which in turn promoted the resulting photocatalytic efficiency toward RhB photodegradation. It is worth noting that the increase in photocatalytic activity of Au-CdS nanocrystals with the increasing shell thickness corresponded well with the result of electron-transfer rate constant variation, which could be realized by the causal relation between electron transfer and hole generation. As the shell thickness of Au-CdS nanocrystals increased, more and more photoexcited electrons transferred from CdS shell to Au core, simultaneously leaving photogenerated holes of an increased amount in CdS shell. The rise in the number of photogenerated holes further led to the enhancement in the resulting photocatalytic performance as observed. For more clarity on this relation, we depicted the correlations of electron-transfer rate constant (k_{et}) and rate constant of RhB photodegradation (k_{RhB}) with the shell thickness of Au-CdS nanocrystals in Figure 4.

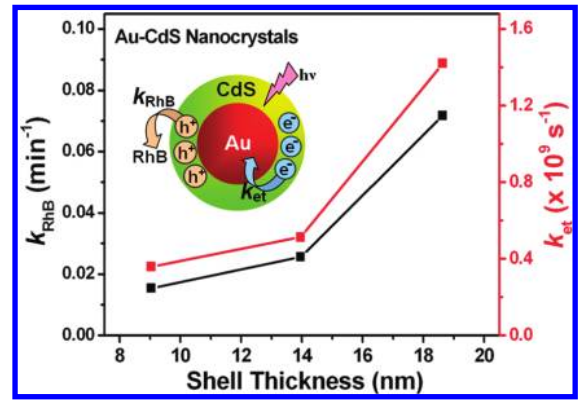

Figure 4. Correlations of electron-transfer rate constant (k_{et}) and rate constant of RhB photodegradation (k_{RhB}) with the shell thickness of Au-CdS nanocrystals.

Further comparative experiments were conducted to demonstrate the superior photocatalytic performance for the present Au-CdS nanocrystals. Four kinds of photocatalysts including N-doped P-25 TiO_2, commercial CdS powders, CdS counterpart, and Au-CdS nanocrystals were used in the photodegradation of RhB under the same experimental conditions. The comparative results were shown in Figure 5a, from which several points can be observed. First, as compared to the relevant commercial products like N-doped P-25 TiO_2 and CdS powders, Au-CdS nanocrystals exhibited superior photocatalytic performance under visible light illumination, demonstrating their potential as an efficient visible-light-driven photocatalyst in relevant redox reactions. Second, Au-CdS nanocrystals performed better toward RhB photodegradation than CdS counterpart, which can be accounted for by the pronounced charge separation that occurred at the interface of Au and CdS. This demonstration addresses the benefit of the present metal−semiconductor core−shell nanocrystals to photocatalytic applications. To further explore the applicability of the as-synthesized Au-CdS nanocrystals in a more practical situation, their photocatalytic performance under natural sunlight was also evaluated. As illustrated in Figure 5b, after exposure to 150 min of daytime sunlight, 90% of RhB was degraded by using Au-CdS nanocrystals, accompanied by an evident decoloration of the resulting solution. This result shows that the present Au-CdS nanocrystals can be used as highly efficient photocatalysts which may practically harvest energy from sunlight. As a final note, the as-prepared Au-CdS nanocrystals did not suffer significant photocorrosive oxidation as deduced from the XPS data. In Figure 5c, both Cd and S XPS spectra of Au-CdS sample exhibit signals corresponding to the bulk CdS with the binding energies of 404.8, 411.6, and 161.8 eV for Cd $3d_{5/2}$, Cd $3d_{3/2}$, and S 2p core levels,

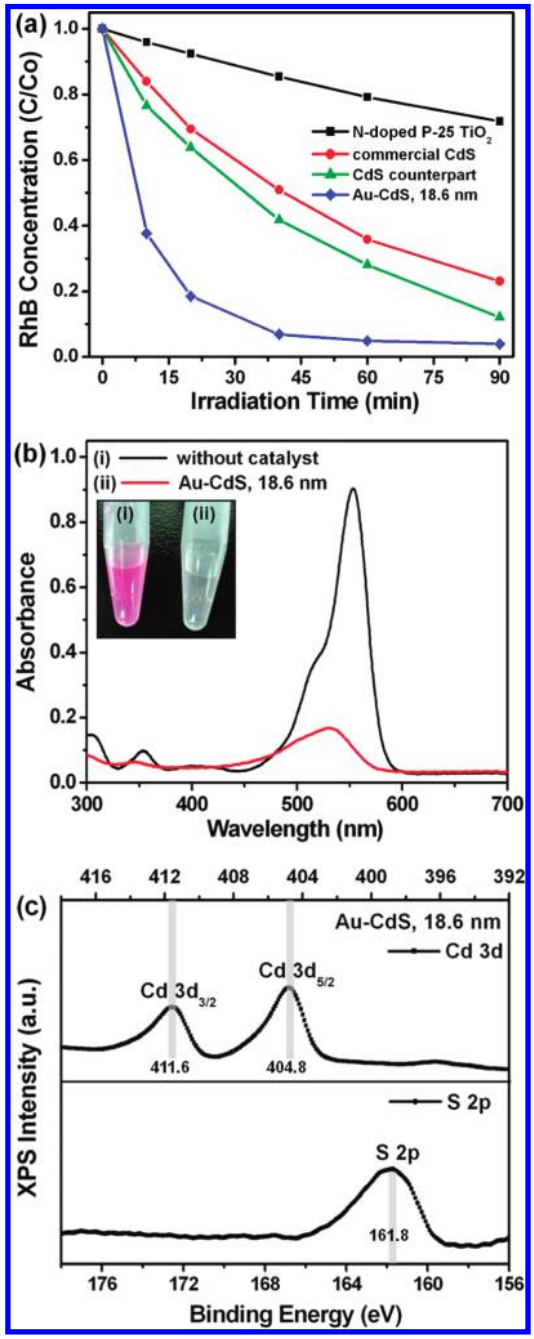

Figure 5. (a) C/C_o versus irradiation time plots for RhB photodegradation in the presence of different photocatalysts. (b) Absorption spectra of RhB solutions after exposure of 150 min of daytime sunlight without any catalyst and in the presence of Au-CdS nanocrystals with the shell thickness of 18.6 nm. Insets: The corresponding solution color. (c) XPS spectra of Cd 3d and S 2p for Au-CdS nanocrystals with the shell thickness of 18.6 nm.

respectively.[29] For the S 2p XPS spectrum, note that no sulfate-related peak at around 168.4 eV, which originated from the photocorrosive oxidation of CdS with oxygen and water,[30] was observed. The absence of sulfate-related peak in the S 2p spectrum indicates that the present Au-CdS nanocrystals exhibited considerably high stability in air, which is important to the durability performance during their use as photocatalysts.

Conclusions

In conclusion, the interfacial charge carrier dynamics for core−shell Au-CdS nanocrystals with various shell thicknesses were investigated and presented. Due to the difference in band structures between Au and CdS, a pronounced photoinduced charge separation took place at the interface of Au and CdS, resulting in the electron-charged Au core and the hole-enriched CdS shell. The electron-charging of Au core in Au-CdS nanocrystals was revealed with the corresponding XPS analysis and photocurrent measurement. Time-resolved PL data showed that a higher electron-transfer rate constant was observed for Au-CdS nanocrystals with thicker CdS shell. On the other hand, the hole-enriched CdS shell of Au-CdS nanocrystals upon light illumination was characterized with a photocatalytic process. The photocatalytic activity of Au-CdS nanocrystals was found to increase with increasing shell thickness, consistent with the result of electron-transfer rate constant variation. The current Au-CdS nanocrystals may find promising photocatalytic applications, especially in the photooxidative decomposition of various organic pollutants such as aldehydes[31] and chlorinated hydrocarbons.[32] The present study also gives rise to a new class of highly efficient metal/semiconductor hybrid photocatalysts which may effectively utilize the solar power.

Acknowledgment. This work was financially supported by the National Science Council of the Republic of China (Taiwan) under grants NSC-97-2221-E-009-073 and NSC-98-2218-E-009-003.

References and Notes

(1) (a) Kamat, P. V. *J. Phys. Chem. C* **2007**, *111*, 2834. (b) Kamat, P. V. *J. Phys. Chem. C* **2008**, *112*, 18737.

(2) (a) Elmalem, E.; Saunders, A. E.; Costi, R.; Salant, A.; Banin, U. *Adv. Mater.* **2008**, *20*, 4312. (b) Costi, R.; Saunders, A. E.; Elmalem, E.; Salant, A.; Banin, U. *Nano Lett.* **2008**, *8*, 637. (c) Chen, W.-T.; Hsu, Y.-T.; *Langmuir* **2010**, *26*, 5918.

(3) (a) Brown, P.; Kamat, P. V. *J. Am. Chem. Soc.* **2008**, *130*, 8890. (b) Farrow, B.; Kamat, P. V. *J. Am. Chem. Soc.* **2009**, *131*, 11124. (c) Williams, G.; Kamat, P. V. *Langmuir* **2009**, *25*, 13869.

(4) (a) Kongkanand, A.; Tvrdy, K.; Takechi, K.; Kuno, M.; Kamat, P. V. *J. Am. Chem. Soc.* **2008**, *130*, 4007. (b) Tak, Y.; Kim, H.; Lee, D.; Yong, K. *Chem. Commun.* **2008**, 4585. (c) Tvrdy, K.; Kamat, P. V. *J. Phys. Chem. A* **2009**, *113*, 3765. (d) Zhang, J.; Bang, J. H.; Tang, C.; Kamat, P. V. *ACS Nano* **2010**, *4*, 387. (e) Chakrapani, V.; Tvrdy, K.; Kamat, P. V. *J. Am. Chem. Soc.* **2010**, *132*, 1228.

(5) (a) Hirakawa, T.; Kamat, P. V. *J. Am. Chem. Soc.* **2005**, *127*, 3928. (b) Zheng, Y.; Zheng, L.; Zhan, Y.; Lin, X.; Zheng, Q.; Wei, K. *Inorg. Chem.* **2007**, *46*, 6980. (c) Zeng, H.; Cai, W.; Liu, P.; Xu, X.; Zhou, H.; Klingshirn, C.; Kalt, H. *ACS Nano* **2008**, *2*, 1661. (d) Chen, H.; Chen, S.; Quan, X.; Yu, H.; Zhao, H.; Zhang, Y. *J. Phys. Chem. C* **2008**, *112*, 9285. (e) Li, J.; Xu, J.; Dai, W.-L.; Fan, K. *J. Phys. Chem. C* **2009**, *113*, 8343.

(6) (a) Wu, G.; Nishikawa, T.; Ohtani, B.; Chen, A. *Chem. Mater.* **2007**, *19*, 4530. (b) Jagadale, T. C.; Takale, S. P.; Sonawane, R. S.; Joshi, H. M.; Patil, S. I.; Kale, B. B.; Ogale, S. B. *J. Phys. Chem. C* **2008**, *112*, 14595. (c) Periyat, P.; Pillai, S. C.; McCormack, D. E.; Colreavy, J.; Hinder, S. J. *J. Phys. Chem. C* **2008**, *112*, 7644.

(7) (a) Zhao, Z.-G.; Miyauchi, M. *Angew. Chem., Int. Ed.* **2008**, *47*, 7051. (b) He, Y.; Li, D.; Xiao, G.; Chen, W.; Chen, Y.; Sun, M.; Huang, H.; Fu, X. *J. Phys. Chem. C* **2009**, *113*, 5254. (c) Frame, F. A.; Carroll, E. C.; Larsen, D. S.; Sarahan, M.; Browningb, N. D.; Osterloh, F. E. *Chem. Commun.* **2008**, 2206. (d) Sun, M.; Li, D.; Li, W.; Chen, Y.; Chen, Z.; He, Y.; Fu, X. *J. Phys. Chem. C* **2008**, *112*, 18076. (e) Cho, I.-S.; Lee, S.; Noh, J. H.; Choi, G. K.; Jung, H. S.; Kim, D. W.; Hong, K. S. *J. Phys. Chem. C* **2008**, *112*, 18393.

(8) Kamat, P. V.; Shanghavi, B. *J. Phys. Chem. B* **1997**, *101*, 7675.

(9) (a) Jing, D.; Guo, L. *J. Phys. Chem. B* **2006**, *110*, 11139. (b) Bao, N.; Shen, L.; Takata, T.; Domen, K.; Gupta, A.; Yanagisawa, K.; Grimes, C. A. *J. Phys. Chem. C* **2007**, *111*, 17527. (c) Shen, S.; Guo, L. *Mater. Res. Bull.* **2008**, *43*, 437. (d) Li, W.; Li, D.; Chen, Z.; Huang, H.; Sun, M.; He, Y.; Fu, X. *J. Phys. Chem. C* **2008**, *112*, 14943.

(10) Lin, G.; Zheng, J.; Xu, R. *J. Phys. Chem. C* **2008**, *112*, 7363.

(11) (a) Bao, N.; Shen, L.; Takata, T.; Domen, K. *Chem. Mater.* **2008**, *20*, 110. (b) Wang, W.; Zhu, W.; Xu, H. *J. Phys. Chem. C* **2008**, *112*, 16754.

(12) (a) Yao, W.-T.; Yu, S.-H.; Liu, S.-J.; Chen, J.-P.; Liu, X.-M.; Li, F.-Q. *J. Phys. Chem. B* **2006**, *110*, 11704. (b) Janet, C. M.; Viswanath, R. P. *Nanotechnology* **2006**, *17*, 5271. (c) Jang, J. S.; Joshi, U. A.; Lee, J. S. *J. Phys. Chem. C* **2007**, *111*, 13280. (d) Li, Y.; Hu, Y.; Peng, S.; Lu,

G.; Li, S. *J. Phys. Chem. C* **2009**, *113*, 9352. (e) Zhang, F.; Wong, S. S. *Chem. Mater.* **2009**, *21*, 4541.

(13) Huang, Y.; Sun, F.; Wang, H.; He, Y.; Li, L.; Huang, Z.; Wu, Q.; Yu, J. C. *J. Mater. Chem.* **2009**, *19*, 6901.

(14) (a) Guan, G.; Kida, T.; Kusakabe, K.; Kimura, K.; Fang, X.; Ma, T.; Abe, E.; Yoshida, A. *Chem. Phys. Lett.* **2004**, *385*, 319. (b) Jing, D.; Guo, L. *J. Phys. Chem. C* **2007**, *111*, 13437. (c) Zong, X.; Yan, H.; Wu, G.; Ma, G.; Wen, F.; Wang, L.; Li, C. *J. Am. Chem. Soc.* **2008**, *130*, 7176. (d) Tak, Y.; Kim, H.; Lee, D.; Yong, K. *Chem. Commun.* **2008**, 4585. (e) Li, G.-S.; Zhang, D.-Q.; Yu, J. C. *Environ. Sci. Technol.* **2009**, *43*, 7079. (f) Kannaiyan, D.; Kim, E.; Won, N.; Kim, K. W.; Jang, Y. H.; Cha, M.-A.; Ryu, D. Y.; Kimc, S.; Kim, D. H. *J. Mater. Chem.* **2010**, *20*, 677.

(15) Chen, W.-T.; Yang, T.-T.; Hsu, Y.-J. *Chem. Mater.* **2008**, *20*, 7204.

(16) (a) Khan, S. U. M.; Al-Shahry, M.; Ingler, W. B., Jr. *Science* **2002**, *297*, 2243. (b) Nakamura, R.; Tanaka, T.; Nakato, Y. *J. Phys. Chem. B* **2004**, *108*, 10617.

(17) Zhang, H.-L.; Evans, S. D.; Henderson, J. R.; Miles, R. E.; Shen, T. *J. Phys. Chem. B* **2003**, *107*, 6087.

(18) Tian, C.; Mao, B.; Wang, E.; Kang, Z.; Song, Y.; Wang, C.; Li, S. *J. Phys. Chem. C* **2007**, *111*, 3651.

(19) Yu, K.; Wu, Z.; Zhao, Q.; Li, B.; Xie, Y. *J. Phys. Chem. C* **2008**, *112*, 2244.

(20) (a) James, D. R.; Liu, Y.-S.; de Mayo, P.; Ware, W. R. *Chem. Phys. Lett.* **1985**, *120*, 460. (b) Posokhov, Y. O.; Ladokhin, A. S. *Anal. Biochem.* **2006**, *348*, 87.

(21) (a) Chae, W.-S.; Ko, J.-H.; Hwang, I.-W.; Kim, Y.-R. *Chem. Phys. Lett.* **2002**, *365*, 49. (b) Sadhu, S.; Chowdhury, P. S.; Patra, A. *J. Lumin.* **2007**, *126*, 387.

(22) (a) Chestnoy, N.; Harris, T. D.; Hull, R.; Brus, L. E. *J. Phys. Chem.* **1986**, *90*, 3393. (b) Chen, W.; Bovin, J.-O.; Joly, A. G.; Wang, S.; Su, F.; Li, G. *J. Phys. Chem. B* **2004**, *108*, 11927.

(23) Lu, S. G.; Xu, Z. K.; Chen, H.; Mak, C. L.; Wong, K. H.; Li, K. F.; Cheah, K. W. *J. Appl. Phys.* **2006**, *99*, 064103.

(24) (a) Kima, D. S.; Park, Y. S. *Chem. Eng. J.* **2006**, *116*, 133. (b) Li, J.; Li, L.; Zheng, L.; Xian, Y.; Jin, L. *Electrochim. Acta* **2006**, *51*, 4942. (c) Sun, S.; Wang, W.; Zhang, L.; Zhou, L.; Yin, W.; Shang, M. *Environ. Sci. Technol.* **2009**, *43*, 2005.

(25) (a) Chen, C.; Zhao, W.; Li, J.; Zhao, J.; Hidaka, H.; Serpone, N. *Environ. Sci. Technol.* **2002**, *36*, 3604. (b) Lei, P.; Chen, C.; Yang, J.; Ma, W.; Zhao, J.; Zhang, L. *Environ. Sci. Technol.* **2005**, *39*, 8466.

(26) Konstantinou, I. K.; Albanis, T. A. *Appl. Catal. B* **2004**, *49*, 1.

(27) (a) Subramanian, V.; Wolf, E. E.; Kamat, P. V. *J. Phys. Chem. B* **2003**, *107*, 7479. (b) Jakob, M.; Levanon, H.; Kamat, P. V. *Nano Lett.* **2003**, *3*, 353. (c) Subramanian, V.; Wolf, E. E.; Kamat, P. V. *J. Am. Chem. Soc.* **2004**, *126*, 4943.

(28) Hirakawa, T.; Kamat, P. V. *Langmuir* **2004**, *20*, 5645.

(29) (a) Antoun, T.; Brayner, R.; Al terary, S.; Fiévet, F.; Chehimi, M.; Yassar, A. *Eur. J. Inorg. Chem.* **2007**, 1275–1284. (b) Hota, G.; Idage, S. B.; Khilar, K. C. *Colloids Surf., A* **2007**, *293*, 5–12.

(30) (a) Reber, J.-F.; Meier, K. *J. Phys. Chem.* **1984**, *88*, 5903. (b) Meissner, D.; Memming, R.; Kastening, B. *J. Phys. Chem.* **1988**, *92*, 3476.

(31) (a) Wang, Y.; Wang, Y.; Meng, Y.; Ding, H.; Shan, Y.; Zhao, X.; Tang, X. *J. Phys. Chem. C* **2008**, *112*, 6620. (b) Wu, X.-F.; Song, H.-Y.; Yoon, J.-M.; Yu, Y.-T.; Chen, Y.-F. *Langmuir* **2009**, *25*, 6438.

(32) Hoffmann, M. R.; Martin, S. T.; Choi, W.; Bahnemann, D. W. *Chem. Rev.* **1995**, *95*, 69.

JP103294C